

Cavity magnomechanics

Xufeng Zhang,¹ Chang-Ling Zou,^{1,2} Liang Jiang,² and Hong X. Tang^{1,2,*}

¹*Department of Electrical Engineering, Yale University, New Haven, Connecticut 06511, USA*

²*Department of Applied Physics, Yale University, New Haven, Connecticut 06511, USA*

(Dated: November 17, 2015)

A dielectric body couples with electromagnetic fields through radiation pressure and electrostrictive forces, which mediate phonon-photon coupling in cavity optomechanics [1]. In a magnetic medium, according to Korteweg-Helmholtz formula [2], magnetostrictive forces should arise and lead to phonon-magnon interaction. Here we report such a coupled phonon-magnon system based on ferrimagnetic spheres, which we term as cavity magnomechanics, by analogy to cavity optomechanics. Coherent phonon-magnon interactions, including electromagnetically induced transparency and absorption, are demonstrated. Excitingly, due to strong hybridization of magnon and microwave photon modes and their high tunability, our platform exhibits new features including parametric amplification of magnons and phonons, triply resonant photon-magnon-phonon coupling and phonon lasing. Our work demonstrates the fundamental principle of cavity magnomechanics and its application as a new information transduction platform based on coherent coupling between photons, phonons and magnons.

Mechanical oscillators have been recently widely studied as a transducer mediating the coherent signal conversion between different systems [1]. Particularly, radiation force [3–7], electrostatic force [8–10] and piezoelectric force [11, 12] have been utilized for coupling phonon with optical or microwave photons. Such interaction mechanisms lead to the fast development of a variety of cavity electro- and opto-mechanical systems [1], but they all intrinsically lack good tunability. The magnetostrictive force [2] provides an alternative mechanism to allow a different information carrier – magnon – to couple with phonon. Magnon is a collective excitation of magnetization, whose frequency can be tuned at will by adjusting bias magnetic field [13–15]. The magnetostrictive interaction has been long overlooked for information processing as it is negligibly weak in commonly used dielectric or metallic materials. However, in magnetic materials such as yttrium iron garnet (YIG, $\text{Y}_3\text{Fe}_5\text{O}_{12}$), the magnetostrictive force becomes dominant, which provides a great opportunity to establish an highly tunable hybrid system for coherent information processing. Thanks to

the excellent material property of YIG, the magnomechanical system can be further integrated with opto- or electro-mechanical elements, providing an excellent platform for quantum state transfer among different physical systems.

Here, we demonstrate an intriguing cavity magnomechanical system in which magnon couples with phonon through magnetostrictive interaction, resulting in hallmark coherent phenomena such as magnomechanically induced transparency/absorption (MMIT/MMIA) and magnomechanical parametric amplification (MMPA). During such processes, magnons are in the hybridized state with cavity microwave photons as they are strongly coupled to each other [16–20]. Therefore coherent signal conversions among these three different information carriers are realized in a single device. The magnetic field dependence of magnon provides our system with unprecedented tunability compared with opto- or electro-mechanical systems. Moreover, the great flexibility of this system allows us to achieve triple-resonance among magnon, phonon and photon, which drastically enhances the magnomechanical interaction. The principles demonstrated in our room temperature experiments can be readily applied to the quantum regime at millikelvin temperature, opening up great opportunities in various applications, such as tunable microwave filter and amplifier [21], long-lifetime quantum memories [22], microwave-to-optics conversion [9].

Magnetostrictive interaction

The device used in our experiments is schematically shown in Fig. 1A. The key component is a highly polished single crystal YIG sphere glued to the end of a silica fiber for supporting purpose (Fig. 1B). With an external magnetic field H biased along z direction, a uniform magnon mode resonates in the YIG sphere at frequency $\omega_m = \gamma H$, where γ is the gyromagnetic ratio. The YIG sphere is also an excellent mechanical resonator (Fig. 1C) thanks to its superior material and geometrical properties. The varying magnetization induced by the magnon excitation inside the YIG sphere causes deformation of its spherical geometry (and vice versa), introducing the coupling between magnon and phonon modes (Fig. 1D). Considering the large frequency mismatch between the magnon and the phonon modes (gigahertz v.s. megahertz) with our experiment parameters, a strong parametric drive is used to compensate their frequency difference. In this case, the system is described by an radiation pressure-like, dispersive interaction Hamiltonian $\mathcal{H} = \hbar g_{\text{mb}} \hat{m}^\dagger \hat{m} (\hat{b} + \hat{b}^\dagger)$, where \hbar is the reduced Planck's constant, \hat{b} (\hat{m}) is the

* To whom correspondence should be addressed. E-mail: hong.tang@yale.edu

boson operator of the phonon (magnon) mode, and g_{mb} is the single magnon-phonon coupling strength.

Spheroidal phonon modes

The magnetostrictive coupling strength is determined by the mode overlap between the uniform magnon mode and the phonon modes. In a YIG sphere, there exist various phonon modes, each with a different displacement profile and consequently a different coupling strength with the magnon mode. Figure 2A plots the typical profiles of the lowest order spheroidal phonon modes S_{1,l,m_a} (l and m_a are the angular and azimuthal mode numbers, respectively), among which the $S_{1,2,2}$ mode shows the highest coupling strength when the bias field is along the direction of maximum displacement (Fig. 2B). Therefore in our experiments we focus only on the $S_{1,2,2}$ mode. Although a YIG sphere with a smaller diameter is favorable for achieving larger coupling strengths (Fig. 2B), it also results in a higher frequency for the phonon mode (Fig. 2C), which in turn leads to lower responsivity to the parametric drive, so a trade-off has to be made when choosing the sphere size. In our experiments, a 250- μ m-diameter YIG sphere is used, corresponding to a phonon frequency $\omega_b/2\pi = 11.42$ MHz and a coupling strength $g_{mb}/2\pi \leq 9.9$ mHz. With an external drive of 0 dBm, the linear magnon-phonon coupling can be enhanced to around 30 kHz, which is two orders of magnitude larger than the phonon dissipation rate κ_b .

Magnetostriction mediates the coupling between magnons and photons. However, in order to achieve coherent magnon-phonon coupling, it is further required that phonon mode should have relatively long lifetime. Single crystal YIG has a garnet structure that is known to exhibit very low mechanical damping and therefore supports a material-limited phonon lifetime over a millisecond [23]. The supporting fiber that is glued to the YIG sphere reduces the phonon lifetime (Fig. 2D). In our experiments, the measured linewidth of $S_{1,2,2}$ phonon mode with a 125- μ m-diameter supporting fiber is $2\kappa_b/2\pi = 300$ Hz, which is sufficiently small for observing coherent magnon-phonon coupling phenomena.

Coherent magnomechanical interaction

Figure 1E plots the schematics of our measurement setup at room temperature ambient condition. The YIG sphere is placed inside a three-dimensional microwave cavity (Fig. 1A). A weak probe signal is sent into the cavity through a coaxial probe, and by sweeping its frequency ω_s and measuring the reflection, we can infer the interaction among photon, magnon and phonon inside the cavity. The YIG sphere is positioned at the maximum microwave magnetic field of the cavity TE_{011} mode, which resonates at $\omega_a/2\pi = 7.86$ GHz. By controlling the bias magnetic field, we tune the magnon close to resonance with the cavity photon mode. This leads to the hybridization between magnon and photon [16–19], which shows up in the reflection spectrum as a pair of split normal modes (Fig. 1F). Because each of the two hybrid modes con-

tains magnon components, it coherently couples with the phonon modes when the cavity is parametrically driven by a strong microwave signal at ω_d .

We first study the coherent magnomechanical coupling for each individual hybrid mode by applying an off-resonance microwave drive. In this case, the cavity magnomechanical system can be described by

$$\mathcal{H}_{mb} = \hbar g_{mb}(\hat{b} + \hat{b}^\dagger)(\cos^2 \theta \hat{A}_+^\dagger \hat{A}_+ + \sin^2 \theta \hat{A}_-^\dagger \hat{A}_-), \quad (1)$$

where the two hybrid modes interact with the phonon mode independently. Here, $\hat{A}_+ = \cos \theta \hat{a} + \sin \theta \hat{m}$ and $\hat{A}_- = -\sin \theta \hat{a} + \cos \theta \hat{m}$ are quantized boson operators for hybridized excitations constituted by magnon and microwave photon (\hat{a}), with $\theta = \frac{1}{2} \arctan \frac{2g_{ma}}{\Delta_{ma}}$ varies with photon-magnon coupling strength g_{ma} and photon-magnon detuning $\Delta_{ma} = \omega_m - \omega_a$. In our system, both the magnon and the cavity photon modes have a relatively narrow linewidth ($2\kappa_m/2\pi = 1.12$ MHz and $2\kappa_a/2\pi = 3.35$ MHz). As a result, the hybrid mode linewidth is well below the phonon frequency, leading our system deep inside the resolved sideband regime, by analogy with optomechanical systems [1]. In this case, the nonlinear interaction can be converted either into the linear beam splitter model $\hbar(G_\pm \hat{A}_\pm^\dagger \hat{b} + G_\pm^* \hat{A}_\pm \hat{b}^\dagger)$ or the parametric oscillator model $\hbar(G_\pm \hat{A}_\pm^\dagger \hat{b}^\dagger + G_\pm^* \hat{A}_\pm \hat{b})$ with the presence of an external drive, where $G_\pm = A_{\pm,ss} g_{mb} (1 \mp \cos 2\theta)/2$ is the enhanced coupling strength. Here, $A_{\pm,ss}$ is the steady state amplitude of the hybrid mode, corresponding to the effective pumping of the microwave drive on magnon due to the magnon-photon hybridization.

Figures 3A and B plot the measured reflection spectra for a series of bias magnetic fields with a microwave drive at a fixed frequency ω_d . To avoid the influence of the other hybrid mode, the driving signal is red (blue) detuned for the lower (upper) hybrid mode, as illustrated by the top insets. For the red-detuned drive, the power is held constant at 26 dBm. In the spectra, the broad Lorentzian-shaped resonance dip corresponds to the hybrid mode \hat{A}_- , while the very sharp modification of the spectra at the two-photon detuning $\Delta_{sd} = \omega_b$ is evidence of coherent magnomechanical interaction. The zoomed-in spectra in Fig. 3A show that these phonon-induced resonances have a Fano-like shape that varies with bias magnetic field. When the drive-resonance detuning $\Delta_{d-} = \omega_d - \omega_- = -\omega_b$, the Fano-like resonance changes into a symmetric Lorentzian-shaped transparency peak (MMIT). In contrast, the Fano-like resonances in the spectra for the blue-detuned drive (with a constant power of 22 dBm) show an opposite symmetry (Fig. 3B). When the drive is blue detuned to $\Delta_{d+} = \omega_d - \omega_+ = \omega_b$, such a resonance becomes a Lorentzian-shaped absorption dip (MMIA).

One distinct advantage of magnon is that its frequency is determined by the external bias magnetic field and therefore can be conveniently tuned in a broad range. By varying Δ_{ma} , the percentage of magnon component in the hybrid mode changes. Therefore, the hybrid mode

experiences different effective dissipation rate, external coupling rate, as well as effective coupling strength with the phonon mode. As a result, the coherent magnomechanical interaction is magnetically controllable, which can be quantified by the dependence of the cooperativity $C = G_{\pm}^2 / \kappa_{\pm} \kappa_b$ on the bias magnetic field. The measured C - H relation is plotted in Fig. 3D. For each measurement under a specific bias condition, the drive frequency is detuned from the hybrid mode by $\Delta_{d\pm} = \pm\omega_b$, as indicated by the crosses in Fig. 3C, while the driving power is fixed constant at 30 dBm. We can see there exists an optimal condition for a maximum C , as a the result of the competition between the magnon and photon components in the hybrid mode: more magnon component yields stronger magnetostrictive coupling, while more photon component leads to a higher driving efficiency. From these measurement results we can extract the magnon-phonon coupling strength $g_{mb}/2\pi = 4.1$ mHz, in accordance with our theoretical prediction (Fig. 2B).

Triply resonant cavity magnomechanics

The great flexibility of our system leads to tremendous advantages. For instance, it allows us to work in the interesting triple-resonance condition, where both maximum hybridized modes simultaneously couple with the phonon mode, as described by

$$\mathcal{H}_{mb} = \frac{1}{2} \hbar g_{mb} (\hat{b} + \hat{b}^\dagger)(\hat{A}_+^\dagger \hat{A}_- + \hat{A}_-^\dagger \hat{A}_+). \quad (2)$$

By adjusting the direction of bias field or the position of the YIG sphere inside the cavity, we can tune the hybrid mode splitting to match the phonon frequency ω_b . In this case, both the drive and probe photons can be applied on-resonance with the hybrid modes (top inset of Figs. 4A and B), resulting in a drastically enhanced magnomechanical coupling. For the red-detuned drive, the transparency windows at various driving powers are plotted in Fig. 4A. In addition to the red shift of the center frequency, the linewidth of the transparency windows exhibits a clear linear dependence on the driving power (Fig. 4C, red squares). With a driving power of only 8.0 dBm, the linewidth increases from its intrinsic value 0.62 kHz to 2.12 kHz, corresponding to a cooperativity $C = 2.4$. As a comparison, a driving power of 34 dBm is used to achieve the same cooperativity when the drive is applied off-resonance, indicating the drastic enhancement of the magnomechanical interaction induced by the triple-resonance condition. The reflection signal for the blue detuning situation is plotted in Fig. 4B at various driving powers. As the driving power increases, the center frequency of the small phonon-induced resonance inside the hybrid mode is blue shifted, and its linewidth linearly decreases (Fig. 4C, blue circles).

A direct comparison of Figs. 4A and B reveals distinctly different spectral lineshapes of the phonon-induced resonances. The same as in the case of off-resonance drive, we observed MMIT for the red-detuned drive in the triply resonant system, with the peak height

and linewidth of the transparency window increasing with the driving power. While for the blue-detuned drive, we observed the transition from MMIA to MMIT, and then to MMPA and eventually self-sustained oscillation as we increase the driving power. These observations lead to a unified explanation about the modified spectral lineshape (which is not limited to the triple resonance situation): the coupling with phonon introduces additional dissipation and phase shift to the hybridized modes and therefore changes their lineshapes. With the presence of a parametric drive, the effective dissipation rate of the hybrid mode is modified from κ to $\kappa(1 \pm C)$, which increases for the red-detuned drive while decreases for blue-detuned drive. Given a fixed external coupling rate κ_e , the on-resonance reflectivity of the cavity is

$$r = \frac{1 \pm C - 2 \frac{\kappa_e}{\kappa}}{1 \pm C}. \quad (3)$$

Therefore, depending on the external coupling condition and the driving power, the reflection spectra lineshape varies among MMIT, MMIA or MMPA.

The measured on-resonance reflectivity for an under-coupled hybrid mode agrees well with our theoretical model (Fig. 4D). For the red-detuned drive, the increasing linewidth with elevated driving power causes the mode further under-coupled and therefore the on-resonance reflectivity increases. On the contrary, for the blue-detuned situation, the decreasing linewidth first leads to critical coupling and then over coupling condition, yielding a dip in the reflectivity followed by a rapid increase which diverges as $C \approx 1$ at a driving power of 6.2 dBm. The deviation of the measured reflectivity from the theoretical prediction can be attributed to thermal instability or gain-bandwidth-product limitation, which also limit the highest measurable parametric gain to 3 dB. When the hybrid mode is tuned to over coupled, the increase of the parametric gain with the driving power is more gradual, and therefore a much higher parametric gain up to 25 dB is achieved before reaching instability (Fig. 4E). The observed MMPA is similar to the electromechanical parametric amplifiers [24] but with unprecedented tunability. Further increasing the driving power leads the system into the instable regime where the phonon mode experiences self-sustained oscillation. The threshold behavior of the measured emission power from the Stokes sideband, as shown by the inset of Fig. 4D, indicates the onset of the phonon lasing [25].

Conclusion

The demonstration of the coherent magnon-phonon interaction, including the MMIT (MMIA) and MMPA, provides a versatile platform for the coherent information processing. Besides, as YIG also possesses great optical properties such as low optical loss and optomagnetic nonreciprocity, our study shows great potential for integrating different systems, including microwave, optical, mechanical and magnonic systems, in a single device and realizing information inter-conversion among these dif-

ferent information carriers. Distinguished from opto- or electro-mechanical systems, our cavity magnomechanical system shows high level of tunability which allows the resonance be externally controlled in a wide frequency range. Moreover, such a complex system is compatible

with superconducting quantum circuits [26]. All of these are not only crucial for realizing long desired functions such as microwave-to-optical conversion [9–11, 27, 28], but also provide a flexible platform that intrigues the fundamental study of exotic magnetic excitations.

-
- [1] M. Aspelmeyer, T. J. Kippenberg, F. Marquardt, Cavity optomechanics. *Rev. Mod. Phys.* **86**, 1391–1452 (2014).
 - [2] M. Zahn. Derivation of the Korteweg-Helmholtz electric and magnetic force densities including electrostriction and magnetostriction from the quasistatic Poynting’s theorems. In *2006 IEEE Conf. Electr. Insul. Dielectr. Phenom.*, 186–189. IEEE (2006).
 - [3] M. Li *et al.*, Harnessing optical forces in integrated photonic circuits. *Nature* **456**, 480–484 (2008).
 - [4] Y.-S. Park, H. Wang, Resolved-sideband and cryogenic cooling of an optomechanical resonator. *Nature Phys.* **5**, 489–493 (2009).
 - [5] S. Weis *et al.*, Optomechanically induced transparency. *Science* **330**, 1520–1523 (2010).
 - [6] A. H. Safavi-Naeini *et al.*, Electromagnetically induced transparency and slow light with optomechanics. *Nature* **472**, 69–73 (2011).
 - [7] J. T. Hill, A. H. Safavi-Naeini, J. Chan, O. Painter, Coherent optical wavelength conversion via cavity optomechanics. *Nat. Commun.* **3**, 1196 (2012).
 - [8] J. D. Teufel *et al.*, Circuit cavity electromechanics in the strong-coupling regime. *Nature* **471**, 204–208 (2011).
 - [9] R. W. Andrews *et al.*, Bidirectional and efficient conversion between microwave and optical light. *Nature Phys.* **10**, 321–326 (2014).
 - [10] T. Bagci *et al.*, Optical detection of radio waves through a nanomechanical transducer. *Nature* **507**, 81–85 (2014).
 - [11] J. Bochmann, A. Vainsencher, D. D. Awschalom, A. N. Cleland, Nanomechanical coupling between microwave and optical photons. *Nature Phys.* **9**, 712–716 (2013).
 - [12] L. Fan, K. Y. Fong, M. Poot, H. X. Tang, Cascaded optical transparency in multimode-cavity optomechanical systems. *Nat. Commun.* **6**, 5850 (2015).
 - [13] A. A. Serga, A. V. Chumak, B. Hillebrands, YIG magnonics. *J. Phys. D. Appl. Phys.* **43**, 264002 (2010).
 - [14] B. Lenk, H. Ulrichs, F. Garbs, M. Münzenberg, The building blocks of magnonics. *Phys. Rep.* **507**, 107–136 (2011).
 - [15] A. V. Chumak, V. I. Vasyuchka, A. A. Serga, B. Hillebrands, Magnon spintronics. *Nature Phys.* **11**, 453–461 (2015).
 - [16] Y. Tabuchi *et al.*, Hybridizing ferromagnetic magnons and microwave photons in the quantum limit. *Phys. Rev. Lett.* **113**, 083603 (2014).
 - [17] X. Zhang, C.-L. Zou, L. Jiang, H. X. Tang, Strongly coupled magnons and cavity microwave photons. *Phys. Rev. Lett.* **113**, 156401 (2014).
 - [18] M. Goryachev *et al.*, High-cooperativity cavity QED with magnons at microwave frequencies. *Phys. Rev. Appl.* **2**, 054002 (2014).
 - [19] L. Bai, M. Harder, Y. P. Chen, X. Fan, J. Q. Xiao, C.-M. Hu, Spin pumping in electro-dynamically coupled magnon-photon systems. *Phys. Rev. Lett.* **114**, 227201 (2015).
 - [20] G. Kurizki *et al.*, Quantum technologies with hybrid systems. *Proc. Natl. Acad. Sci.* **112**, 3866–3873 (2015).
 - [21] N. Bergeal *et al.*, Phase-preserving amplification near the quantum limit with a Josephson ring modulator. *Nature* **465**, 64–68 (2010).
 - [22] V. Fiore *et al.*, Storing optical information as a mechanical excitation in a silica optomechanical resonator. *Phys. Rev. Lett.* **107**, 133601 (2011).
 - [23] R. LeCraw, E. Spencer, E. Gordon, Extremely low loss acoustic resonance in single-crystal garnet spheres. *Phys. Rev. Lett.* **6**, 620–622 (1961).
 - [24] F. Massel *et al.*, Microwave amplification with nanomechanical resonators. *Nature* **480**, 351–354 (2011).
 - [25] E. G. Spencer, R. C. LeCraw, Magnetoacoustic resonance in yttrium iron garnet. *Phys. Rev. Lett.* **1**, 241–243 (1958).
 - [26] Y. Tabuchi *et al.*, Coherent coupling between a ferromagnetic magnon and a superconducting qubit. *Science* **349**, 405–408 (2015).
 - [27] S. Barzanjeh, M. Abdi, G. J. Milburn, P. Tombesi, D. Vitali, Reversible optical-to-microwave quantum interface. *Phys. Rev. Lett.* **109**, 130503 (2012).
 - [28] Y.-D. Wang, A. A. Clerk, Using interference for high fidelity quantum state transfer in optomechanics. *Phys. Rev. Lett.* **108**, 153603 (2012).

ACKNOWLEDGEMENTS

We thank N. Zhu for gluing the YIG sphere to the silica fiber. This work was supported by DARPA MTO/MESO program (N66001-11-1-4114). C.Z., L.J. and H.X.T. acknowledge support from LPS through an ARO grant (W911NF-14-1-0563) and Packard Foundation. L.J. also acknowledges support from the Alfred P. Sloan Foundation.

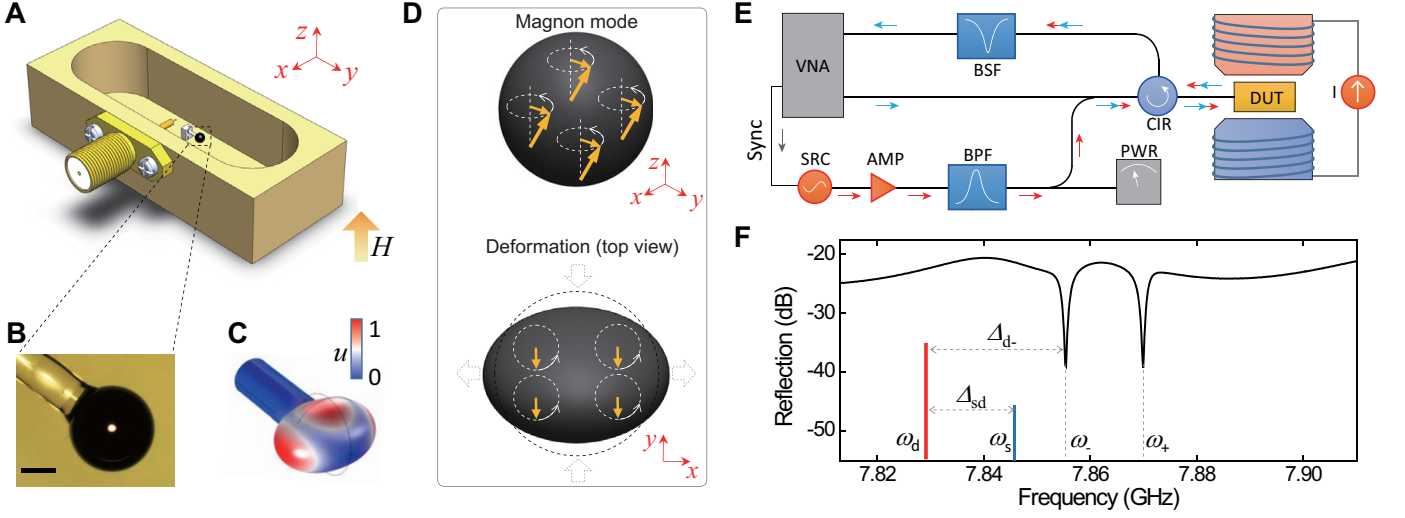


Figure 1. Device schematic and measurement setup. (A) Schematic of the device that consists of a three-dimensional copper cavity (only bottom half is shown) and a YIG sphere. The YIG sphere is placed near the maximum microwave magnetic field (along y direction) of the cavity TE_{011} mode. A uniform external magnetic field (H) is applied along z direction to bias the YIG sphere for magnon-photon coupling. (B) Optical image of the highly polished $250\text{-}\mu\text{m}$ -diameter YIG sphere that is glued to a $125\text{-}\mu\text{m}$ -diameter supporting silica fiber. The gluing area is minimized to reduce the contact damping to the phonon mode. Scale bar: $100\text{ }\mu\text{m}$. (C) Simulated mechanical displacement (u) of the $S_{1,2,2}$ phonon mode in the YIG sphere which has the strongest magnomechanical interaction with the uniform magnon mode. (D) An intuitive illustration of the magnomechanical coupling. Top panel shows the uniform magnon excitation in the YIG sphere. Bottom panel shows that the magnon-induced magnetization (vertical yellow arrows) causes the deformation (compression along y direction) of the YIG sphere (and vice versa). (E) Schematic illustration of the measurement setup. VNA: vector network analyzer; SRC: microwave source for driving; AMP: microwave amplifier; BPF: bandpass filter; PWR: microwave power meter; CIR: circulator; BSF: bandstop filter; DUT: device-under-test. (F) Black curve: cavity reflection spectrum when magnon is on-resonance with the cavity photon mode. The two dips represent the maximum hybridized modes $\hat{A}_{\pm} = \frac{1}{\sqrt{2}}(\hat{a} \pm \hat{m})$. Red and blue vertical lines indicate the applied drive and probe, respectively. The probe is swept across the hybrid mode resonance. Δ_{sd} : two photon (probe-drive) detuning; Δ_{d-} : drive-resonance detuning.

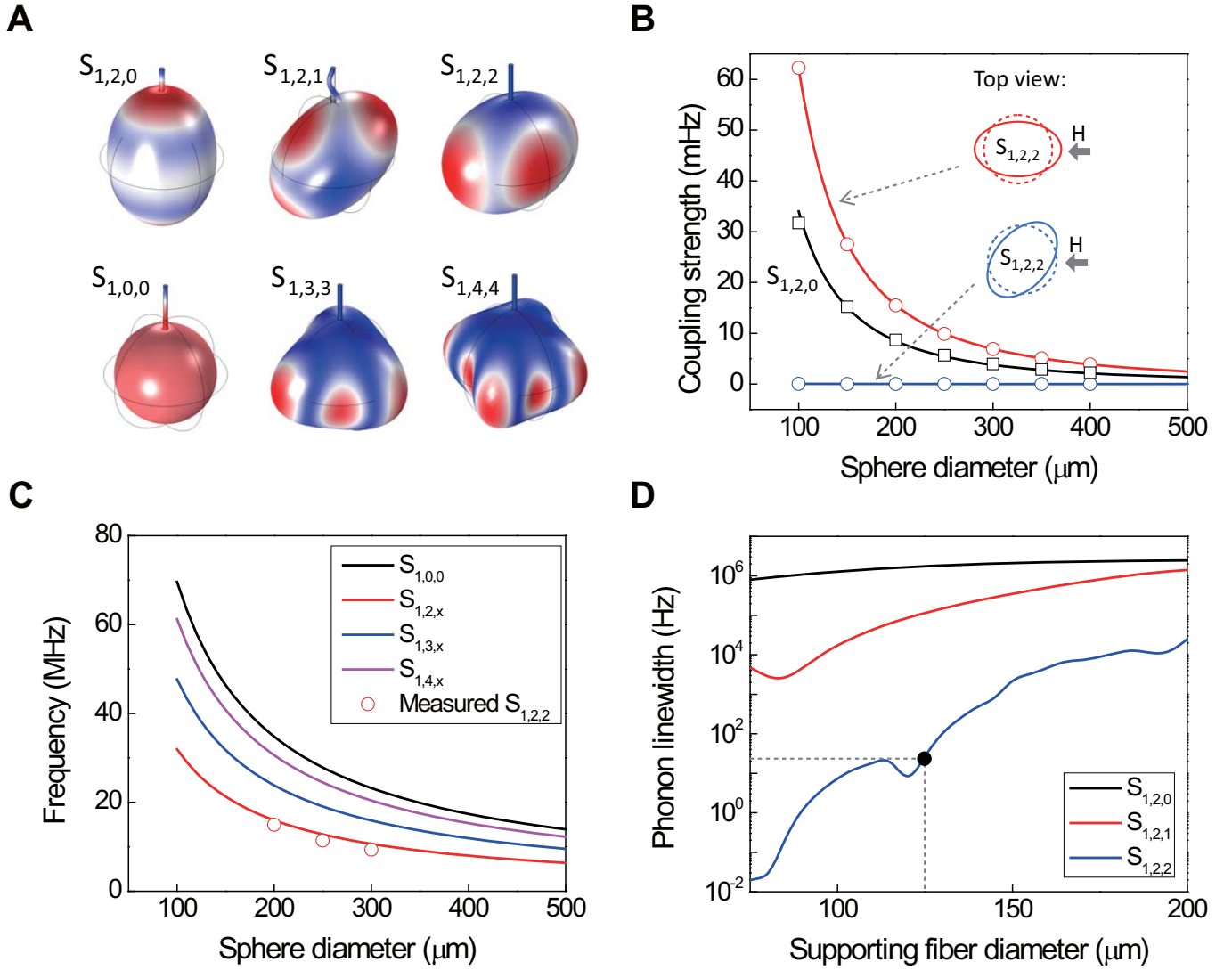


Figure 2. Analysis of the phonon modes and magnetostrictive coupling strengths. (A) Simulated displacement profiles of the low order phonon modes in the YIG sphere (with a small supporting fiber). S_{1,l,m_a} represents the spheroidal mode with a radial mode number of 1, an angular mode number of l , and an azimuthal mode number of m_a . Only one of the $2l + 1$ degenerate modes is plotted for each l . (B) Theoretical prediction of the magnomechanical coupling strength as a function of YIG sphere diameter for the $S_{1,2,0}$ (black) and $S_{1,2,2}$ modes (red and blue, corresponding to different bias field directions). Solid lines are numerical calculations while symbols are analytical fittings. (C) Phonon mode frequency as a function of the YIG sphere diameter. Solid lines are the theoretical calculations, showing an inverse proportional dependence, while red circles are the measurement results. (D) Simulated phonon linewidth due to clamping loss as a function of the supporting fiber diameter for the $S_{1,2,m_a}$ modes. Black dot indicates the experiment parameter, showing an anchor-loss-limited linewidth of 20 Hz.

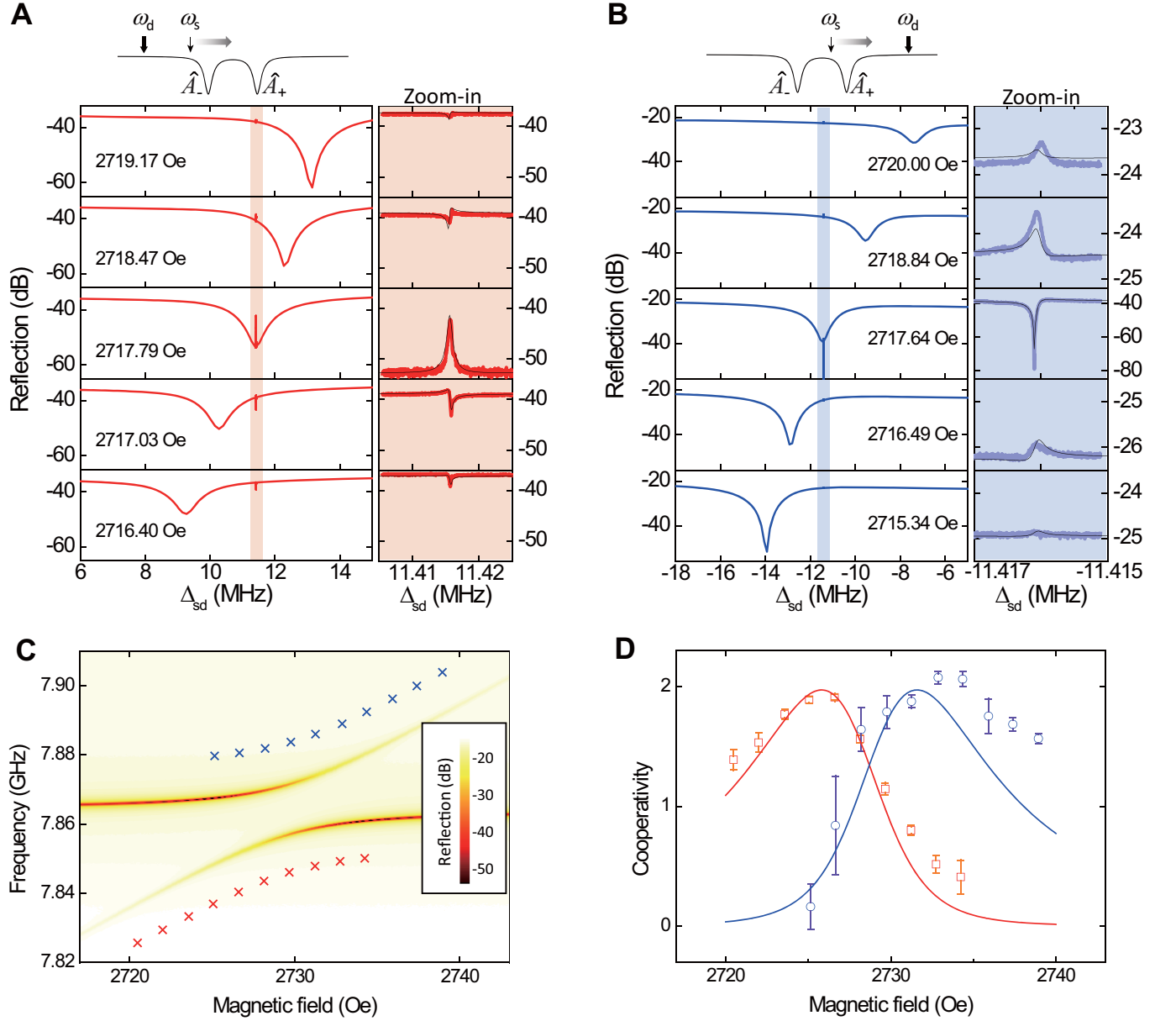


Figure 3. **Tunable magnomechanically induced transparency/absorption.** (A) Measured reflection spectra near the lower hybrid mode \hat{A}_- as a function of the two-photon detuning Δ_{sd} for a series of different bias magnetic fields. The broad dip corresponds to the lower hybrid mode resonance, whose lineshape changes with bias magnetic field because of the change in the ratio between magnon and photon components. A strong (26 dBm) microwave drive is red-detuned with a fixed driving frequency ω_d . A Fano-like narrow resonance line shows up inside the hybrid mode, which turns into a Lorentzian transparency peak when $\Delta_{d-} = -\omega_b$. Zoom-in shows detailed spectra of the magnomechanically induced resonances (shaded area in (A)). (B) Measured reflection spectra near the upper hybrid mode \hat{A}_+ with a blue-detuned strong drive (22 dBm) for various bias magnetic fields. When $\Delta_{d+} = \omega_b$, the magnomechanically induced narrow resonance shows up as a Lorentzian absorption dip. Zoom-in shows detailed spectra of the shaded area in (B). (C) Reflection spectra of the hybrid magnon-photon modes at various bias magnetic fields. The crosses indicate the drive frequency and bias magnetic field used for each data point in (D). (D) The magnomechanical cooperativity as a function of bias magnetic field. For each measurement, the microwave drive is detuned from the hybrid mode by $\Delta_{d\pm} = \pm\omega_b$, while the probe is swept across the hybrid mode resonance. Red squares (blue circles) are for the red (blue) detuning situation. Solid lines in (D) and in the zoom-in of (A) and (B) are theoretical calculations using only a single fitting parameter g_{mb} .

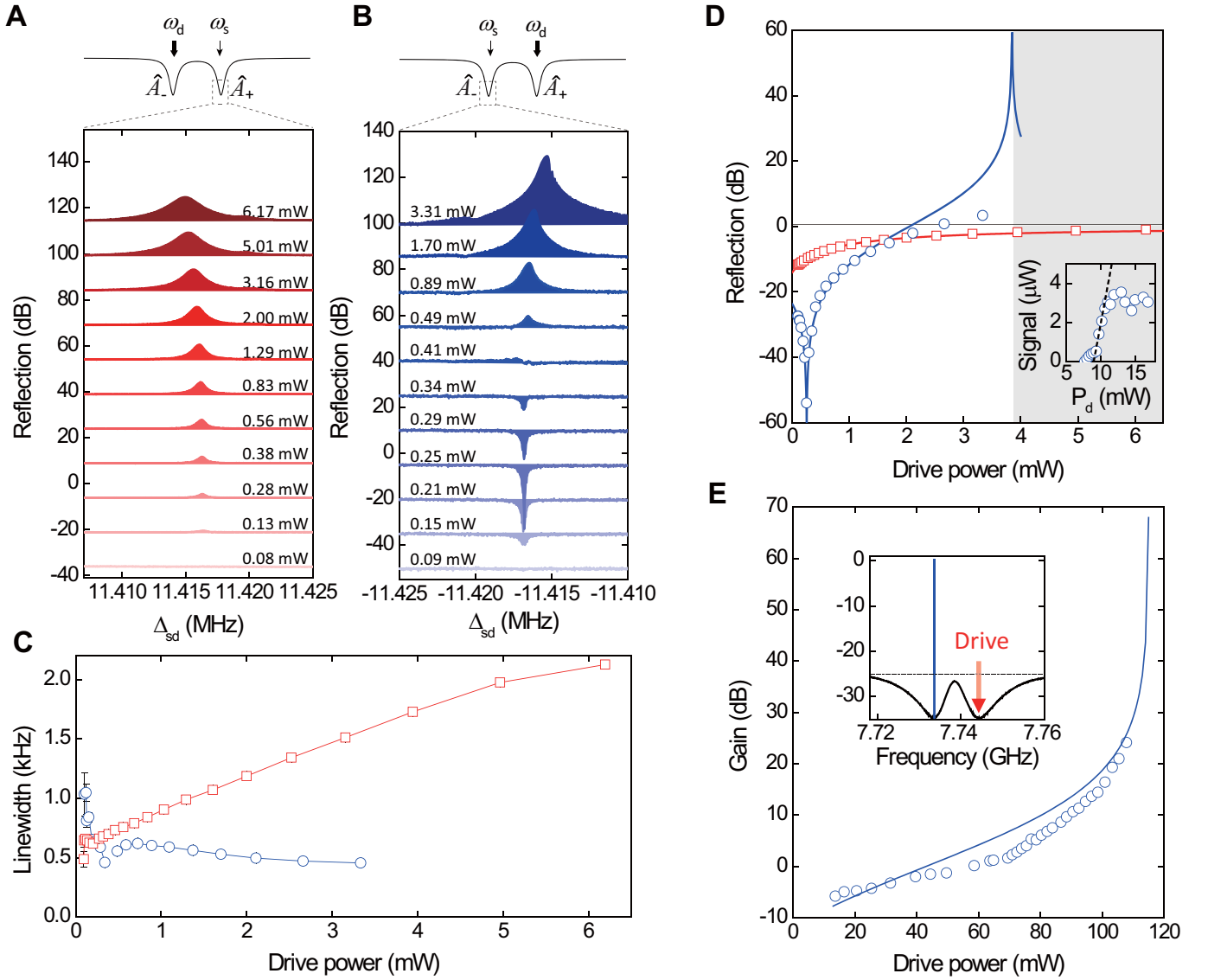


Figure 4. **Enhanced magnomechanical coupling in the triply resonant system.** (A) Magnomechanically induced transparency (MMIT) signal for a red-detuned drive at various driving powers. (B) Magnomechanically induced absorption (MMIA) and magnomechanical parametric gain (MMPA) signal for a blue-detuned drive at various driving powers. (C) The linewidth of the magnomechanically induced resonance as a function of the drive power. (D) Magnomechanical-interaction-modified on-resonance reflectivity of the hybrid mode as a function of the drive power. Shaded area indicates the unstable regime. Inset: Measured power of the Stokes sideband of the driving signal. The threshold behavior indicates the onset of phonon lasing. (E) Magnomechanical parametric gain as a function of the drive power in an over-coupled hybrid system. Inset: Measured reflection spectrum that shows a 25-dB gain. In the main panels of (C)–(E), blue circles (red squares) are for the blue (red) detuning, and solid lines are theoretical calculations.